[18] A. Zouni, H.-T. Witt, J. Kern, P. Fromme, N. Krauß, W. Saenger, P. Orth, *Nature* **2001**, *409*, 739.

[19] Me₄dtne = 1,2-bis(4,7-dimethyl-1,4,7-triazacyclonon-1-yl)ethane was synthesized according to reference [6].

[20] HO₂CPhNIT = 2-(4-carboxyphenyl)-4,4,5,5-tetramethyl-3-oxyimida-zolidin-1-oxide was prepared according to: C. Bätz, P. Amann, H.-J. Deiseroth, L. Dulog, *Liebigs Ann. Chem.* **1994**, 739.

[21] Selected IR stretching frequencies: $\tilde{v} = 1584(m), 1543(m), 1455(m), 1375(s), 1105(s, ClO_4^-), 780(m), 689(m), 624 \text{ cm}^{-1}$ (m). EI mass spectra show two molecular ion peaks at m/z 379 for $[\mathbf{1}]^{2+}$ and 857 for $[\mathbf{1}(ClO_4)]^+$. Elemental analyses (%) calcd for $C_{32}H_{56}Cl_2Mn_2N_8O_{14}$: C 40.13, H 5.86, N 11.71; found: C 38.80, H 5.77, N 11.71.

[22] Crystal structure analysis data for $\mathbf{1}(ClO_4)_2$: $C_{32}H_{56}Cl_2Mn_2N_8O_{14}$, $M_r = 957.63$, monoclinic, $P2_1/c$, $a = 11.6313(4)$, $b = 21.4815(10)$, $c = 16.9454(6)$ Å, $\beta = 108.17(1)°$, $V = 4022.8(3)$ Å³, $Z = 4$, $\rho_{calcd} = 1.581$ Mg m⁻³, $\mu(Mo_{K\alpha}) = 0.836$ mm⁻¹, $F(000) = 2000$; 56074 reflections collected at 100(2) K; 9213 independent reflections; GOF = 1.079; $R = 0.0448$, $wR2 = 0.0827$. CCDC-192780 contains the supplementary crystallographic data for this paper. These data can be obtained free of charge via www.ccdc.cam.ac.uk/conts/retrieving.html (or from the Cambridge Crystallographic Data Centre, 12, Union Road, Cambridge CB2 1EZ, UK; fax: (+44) 1223-336-033; or deposit @ccdc.cam.ac.uk).

[23] Early synthetic attempts at **1** and variants under less mild conditions resulted in complexes wherein decomposition of the NIT moiety took place yielding the imidazolidin-1-oxide radical product, which was evident from inequivalent thermal parameters of O(42) and O(39).

[24] Magnetization of solid $\mathbf{1}(ClO_4)_2$ was measured by using a SQUID magnetometer (MPMS-7, Quantum Design). The molar susceptibilities were corrected for underlying diamagnetism by using tabulated Pascal constants ($X_{dia} = -400 \times 10^{-6}$ cm³ mol⁻¹). The routine JULIUS was used for spin Hamiltonian simulations of the data (C. Krebs, E. Bill, F. Birkelbach, V. Staemmler, unpublished results).

[25] EPR spectra were measured for solutions of **1–3** in acetonitrile with a Bruker ELEXSYS E300 spectrometer with standard or dual-mode cavity and Oxford Instruments ESR910 flow cryostat. Spin-Hamiltonian simulations were performed with the XSOPHE program by G. Hanson et al. that is distributed by Bruker Biospin GmbH.

[26] The latter two complexes are components of an extended and detailed investigation that will be reported in the future. We include only their X-band EPR spectra here for clarity. For **1** in acetonitrile a small degree of dissociation of the bridging carboxylato ligand O₂CPhNIT⁻ from the mother complex $[(Me_4dtne)Mn_2(\mu\text{-O})_2]^{3+}$ is observed. The "impurity" spectra are similar to those in Figure 3a and b and may be easily subtracted from that of intact **1** (shown in Figure 3c). The amount subtracted, integrated to less than 1% by area.

[27] E. Ullman, J. H. Osiecki, D. G. B. Boocock, R. Darcy, *J. Am. Chem. Soc.* **1972**, *94*, 7049.

[28] a) J. E. Wertz, J. R. Bolton, *Electron Spin Resonance*, McGraw-Hill, New York, **1972**; b) P. J. Hore in *Advanced EPR: Applications in Biology and Biochemistry* (Ed.: A. J. Hoff), Elsevier, Amsterdam, **1977**, pp. 405–440.

[29] a) N. M. Atherton, C. J. Winscom, *Inorg. Chem.* **1973**, *12*, 383; b) T. D. Smith, J. R. Pilbrow, *Coord. Chem. Rev.* **1974**, *13*, 173; c) A. Bencini, D. Gatteschi, *EPR of Exchange Coupled Systems*, Springer, Berlin, **1990**.

Real-Time Single-Molecule Imaging of the Formation and Dynamics of Coordination Compounds

Nian Lin,* Alexandre Dmitriev, Jens Weckesser, Johannes V. Barth,* and Klaus Kern*

A current challenge in the field of self-assembled supramolecular nanostructures is the development of strategies for the deliberate positioning of functional molecular species on suitable substrates; this is a crucial aspect in the search for molecular devices.[1] Recent studies revealed that design principles from supramolecular chemistry can be adapted to fabricate unique supramolecular aggregates at surfaces.[2,3] However, to date, mainly hydrogen bonding and electrostatic intermolecular coupling have been successfully exploited to control the ordering of molecular building blocks at low temperatures. These interactions bear the disadvantage of low thermal and mechanical stability. Thus, there is a demand to explore the construction of more rigid supramolecular architectures[4,5] on surfaces. Metal–ligand interactions, which were introduced by Werner at the turn of the 20th century,[6] are recognized as being decisive in molecular recognition and an excellent means for the fabrication of three-dimensional supramolecular arrangements.[7–9] However, the current understanding of the evolution and dynamics of such interactions on surfaces is limited, although their energetics are in a range which lets us expect reaction rates that would permit their direct elucidation at ambient temperature by imaging methods.

For the present investigation conducted on an atomically clean surface we took advantage of ligand systems based on carboxylic acids and transition metals whose characteristics are well understood.[10] Specifically, we addressed metal–ligand bonding of trimesic acid (tma) and Cu atoms. Trimesic acid is a polyfunctional carboxylic acid with threefold symmetry comprised of a phenyl ring and three identical carboxy end groups in the same plane.[11] Its complexation was observed on Cu(100) in ultrahigh vacuum at temperatures in the range 250–300 K following deposition at room temperature. Under these conditions, the carboxylic acid groups are completely deprotonated such that three reactive COO⁻ ligands per tma molecule exist.[12,13] The deprotonation is presumably related to the availability of Cu adatoms at the surface, which are known to exist on Cu(100) in the employed temperature range. The reason behind the presence of Cu adatoms is their continuous evaporation from atomic step

[*] N. Lin, K. Kern, A. Dmitriev, J. Weckesser
Max-Planck-Institut für Festkörperforschung
Heisenbergstrasse 1, 70569 Stuttgart (Germany)
Fax: (+49) 711–689–1662
E-mail: n.lin@fkf.mpg.de
        k.kern@fkf.mpg.de

J. V. Barth, K. Kern
Institut de Physique des Nanostructures
Ecole Polytechnique Fédérale de Lausanne
1015 Lausanne (Switzerland)
E-mail: Johannes.Barth@epfl.ch

📖 Supporting information for this article is available on the WWW under http://www.angewandte.org or from the author.

edges, which accounts for the presence of a two-dimensional lattice gas at the surface. This process can be understood by analogy to the coexistence of gas and condensed phases in bulk systems described by the vapor pressure of a substance. Individual Cu adatoms cannot be resolved in STM images because of their high surface mobility at room temperature.

At appreciable coverages individual molecules appear as equilateral triangles in STM images (Figure 1a), which reflects a flat-lying geometry where the molecule is bound
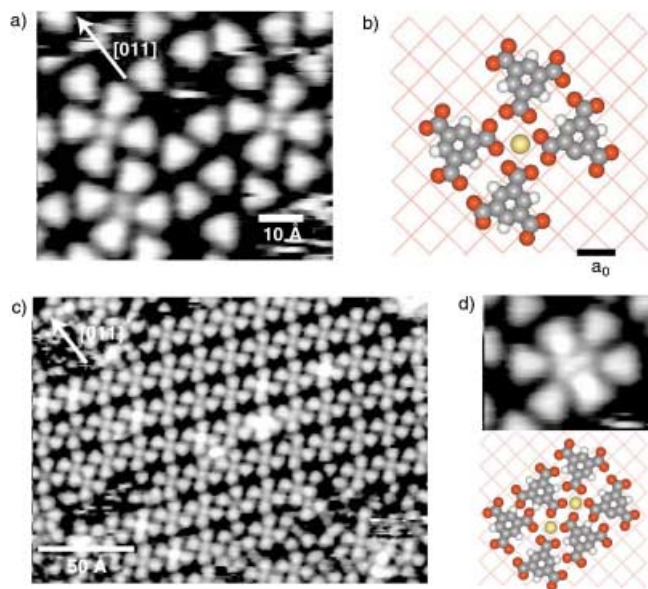
Figure 1. a) STM topograph of trimesic acid adsorbed on a Cu(100) surface at 300 K. The triangular shape reflects a flat-lying adsorption geometry. Cloverleaf-shaped arrangements of four tma molecules with a central protrusion represent $[Cu(tma)_4]^{n-}$ coordination compunds. b) Model for the $[Cu(tma)_4]^{n-}$ configuration with a central Cu atom coordinated by four carboxylate ligands, where carbon atoms are in gray, oxygen atoms in red, hydrogen atoms in white, and Cu adatoms in yellow; the Cu substrate is depicted by the orange lattice, where $a_0 = 3.61$ Å. In agreement with the tunneling data the tma triangles do not point straight to the central site, which indicates a unidentate coordination of the Cu adatom. c) Regular array of $[Cu(tma)_4]^{n-}$ complexes. d) STM image and model of the $[Cu_2(tma)_6]^{n-}$ coordination compound with four unidentate and two *syn,syn* coordination bonds.

with its phenyl ring parallel to the substrate. The symmetry and characteristic side length of approximately 8 Å agrees well with the shape and dimensions of tma.[12] Four distinct orientations with respect to the substrate lattice were found with one of the triangle's corners always pointing along a high-symmetry direction, [011] or [$\bar{0}$11], of the Cu(100) surface. This situation is understood to be a consequence of the occupation of high-symmetry hollow sites at the atomic lattice of the substrate. The data reveal, moreover, that the molecules tend to be arranged in a complementary manner, that is, neighboring tma molecules are oriented antiparallel, and, as such, the close packing at the surface can be explained as a consequence of the space-filling principle. However, this rule is not generally obeyed and arrangements occur where four tma molecules form a cloverleaf structure with a bright protrusion at the center. The formation of the cloverleaf structure is directly related to the density of the Cu adatom

lattice gas.[14] This configuration is associated with a central Cu adatom which is coordinated by the carboxylate ligands from the four surrounding molecules and is hence designated $[Cu(tma)_4]^{n-}$.

A close inspection of the STM image in Figure 1a reveals that the carboxylate ligands of tma do not point straight towards the central protrusion in the compound. This observation demonstrates that the oxygen atoms in the respective COO$^-$ moieties are not equivalent, which indicates a unidentate coordination of the Cu atom as illustrated by the model in Figure 1b. If it is assumed that the tma molecule is in an unrelaxed geometry, the Cu$\cdots$O distance is estimated to be 3 Å, which is substantially larger than the characteristic Cu$\cdots$O distance of approximately 2 Å encountered in three-dimensional copper carboxylates.[10] This Cu$\cdots$O relaxation distance is attributed to the role of the atomic lattice of the substrate, which energetically favors high-symmetry adsorption sites. Moreover, the nature of the coordination bond itself is expected to be modified in the presence of the electrons from the Cu conduction band. Similar effects were encountered in hydrogen-bonded assemblies.[3, 15] Finally, the STM topograph shown in Figure 1c demonstrates that a regular array of $[Cu(tma)_4]^{n-}$ cloverleafs can be obtained.

The square shape of the $[Cu(tma)_4]^{n-}$ configuration with its fourfold coordination is characteristic of Cu^{II} complexes.[16,17] Thus, the cloverleaf arrangement should be considered formally as a $[Cu^{II}(tma)_4]^{10-}$ ion. However, it is important to note that the charge on both the Cu adatoms and the adsorbed tma molecules is strongly affected by the presence of the electrons of the metal surface, which effectively screen any charged adsorbate. A deprotonated tma molecule at the surface should thus not be considered as a $(tma_{ad})^{3-}$ ion, but rather as a neutral tma/Cu(001) complex. As an important consequence, the oxidation state of the central Cu atoms in the $[Cu(tma)_4]^{n-}$ configuration cannot be determined unambiguously. This contrasts the situation encountered with isolated compounds in three dimensions, where the charge is usually balanced by counterions.

Extended one-dimensional or two-dimensional networks, where more than one carboxylate ligand per tma molecule participates in the formation of coordination bonds, were not formed. This is again associated with the influence of the atomic lattice of the substrate, which pins the reactive species in a certain position and orientation to the surface. However, a second compound could be identified close to saturation of the tma monolayer, where two Cu atoms are bound by six tma molecules. An analysis of the corresponding STM data (Figure 1d) reveals that with this $[Cu_2(tma)_6]^{m-}$ configuration four unidentate and two *syn,syn* coordination bonds are present.

The mechanism for the formation of the $[Cu(tma)_4]^{n-}$ compounds could be directly followed by STM measurements at room temperature.[18] The formation of single chemical bonds has been shown before; however, in these studies the bonding was typically induced by manipulating the reactants with the tip of a scanning tunneling microscope at very low temperatures.[19,20] In striking contrast, the reaction proceeds under equilibrium conditions in the present observations. As a consequence, the natural path of a multicomponent chemical

reaction could be characterized: The thermal rotations of single tma molecules at appreciable coverages can be monitored, since surface diffusion is restricted by space limitations. This situation is illustrated by the sequence of images shown in Figure 2, which were taken over a time
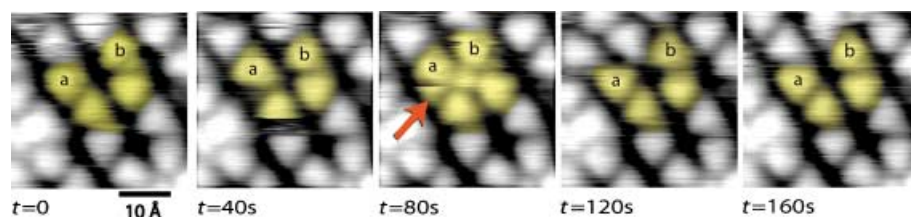
Figure 2. Molecular rotors working as dynamical atom trap: Sequence of STM images revealing the molecular mobility during the association and dissociation of a $[Cu(tma)_4]^{n-}$ cloverleaf over a 160-second time interval. The four tma molecules invloved in the complex formation are artificially highlighted by color. After rotational motions and displacements of tma molecules ($t = 40$ s), a Cu adatom is captured and the coordination compound is formed ($t = 80$ s). A tma molecule which rotated while the image was recorded is marked by an arrow. The coordination bond is subsequently disrupted and the Cu atom disappears again ($t = 120$ s).

interval of 160 s. In the initial frame, the tma molecules marked **a** and **b** change their orientation and position, thus revealing rotation and hopping of single molecules. The characteristic spikes along the scanning direction are caused by motions of the tma molecules occuring while the data were recorded; for example, molecule **a** has switched its orientation from pointing upwards to pointing downwards in the image taken after 80 s (marked by the arrow). Both **a** and **b** are aligned antiparallel with respect to their neighbors at $t = 0$ so as to achieve close packing. Neither of them was in a correct position or orientation for formation of the cloverleaf arrangement. In the second (40 s) and third frames (80 s), **a** and **b** switched orientations, respectively, and the cloverleaf configuration with a central protrusion evolved. This effect is understood to be a result of the capturing of a copper atom diffusing on the surface and the formation of coordinative bonds with the carboxylate ligands of the tma molecules, that is, an association reaction leading to a $[Cu(tma)_4]^{n-}$ complex took place. The Cu atom can exclusively be resolved when it is held by four carboxylate ligands, otherwise its high surface mobility makes STM imaging impossible. The subsequent frame ($t = 120$ s) reveals that the dissociation reaction readily takes place under the same conditions, which indicates that thermal motions or collisions with other molecules are sufficent to disrupt the metal–ligand bond. These observations reveal that molecular rotors (namely, the spinning tma molecules) with functional end groups can operate as a dynamical trap for diffusing Cu adatoms. The formation of the complex is only feasible when four tma molecules switch to the appropriate mutual orientation and snatch a Cu atom passing by at the crucial moment. In marked contrast to $[Cu(tma)_4]^{n-}$, the $[Cu_2(tma)_6]^{n-}$ species was found to be stable under the employed conditions.

Quantitative information on the lifetime and formation of the compounds was obtained from measurements made at low concentrations, where both Cu adatoms and individual tma molecules are highly mobile on the surface. Accordingly, no isolated species can be observed. However, as demonstrated

by the STM image in Figure 3, single or small groups of compounds can be readily resolved. That is, the $[Cu(tma)_4]^{n-}$ configuration is stationary and can be imaged until it eventually dissociates.[21] The lifetime of the cloverleaf arrangements depends strongly on the local environment. For example, the average lifetime with two neighboring compounds (ellipse in Figure 3) is typically more than three times longer than that of an isolated species (circle in Figure 3). This observation suggests the two species have different reactivity, that is, two neighboring species are more stable than isolated ones. Since both measurements were made simultaneously at the same temperature this must be associated with steric effects. As indicated in Figure 3 (tma molecules are marked by arrows), the movement of adjacent molecules in neighboring complexes is impeded so that they experience
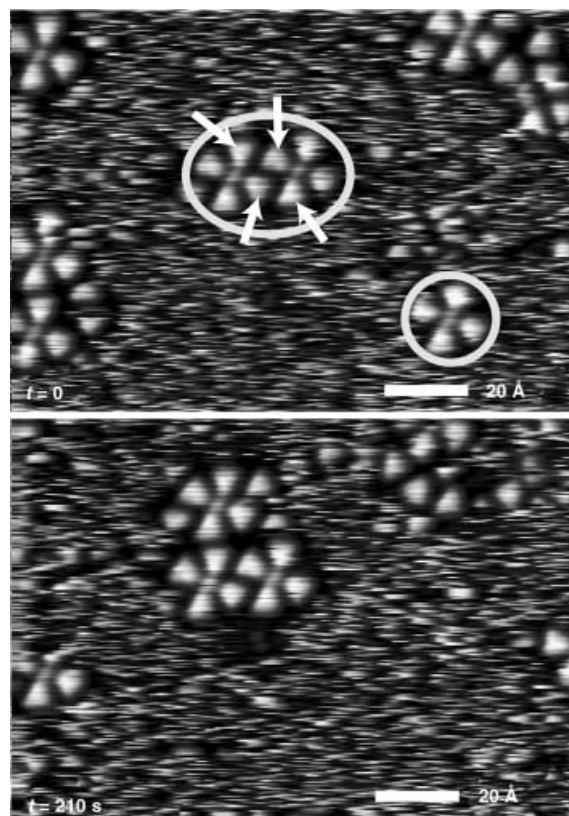
Figure 3. Observation of both isolated and small aggregates of $[Cu(tma)_4]^{n-}$ complexes for low coverages at room temperature. Freely transporting and spinning tma molecules coexist on the surface with copper adatoms, which were not imaged by STM. The characteristic spikes along the scanning direction were caused by those moving tma molecules, while the dark shadows surrounding the stationary $[Cu(tma)_4]$ compounds are areas where free molecules are not present. The lifetime of the isolated compounds (marked by a circle) was determined by sequential imaging of the same area. Aggregates of several compounds such as that marked by the ellipse have increased lifetime because of the hindered motion of neighboring molecules (marked by arrows).

higher energy barriers for rotation or migration. This hindering effect thus indirectly reduces the probability of dissociation. Similarly increased lifetimes were observed for compounds at step edges, where the steps act as the hindrance. In the extreme case a $[Cu(tma)_4]^{n-}$ compound in a regular array (as shown in Figure 1c) has never been observed to dissociate during our measurements, that is, over 5 h. Lifetimes of the $[Cu(tma)_4]^{n-}$ complexes at room temperature in different environments are compiled in Table 1.

Table 1. Average lifetime of $[Cu(tma)_4]^{n-}$ complexes in different local chemical environments at 300 K.

	Isolated on terrace	At step edge	Two neighboring	Saturated layer
lifetime [s]	34 ± 5	87 ± 5	120 ± 5	> 18000

The average lifetime of an isolated cloverleaf was determined from an analysis of STM sequences with 100 frames recorded at room temperature with high scanning velocities (9 s per frame) to be 34 ± 5 s. The inverse of this value corresponds to the mean dissociation rate. In a similar way, dissociation rates at reduced temperatures have been determined; the entire result is plotted in the Arrhenius representation in Figure 4. The data points fall on a straight line whose
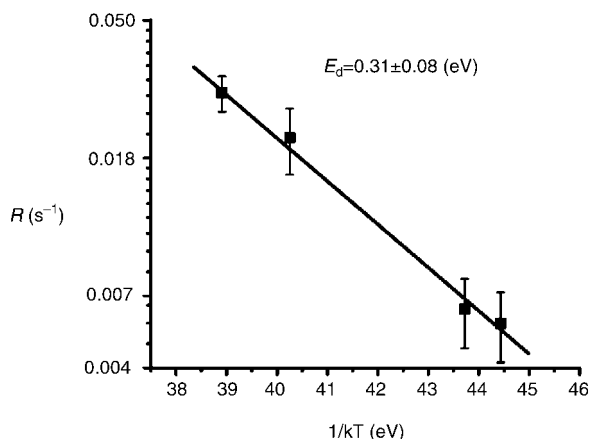
Figure 4. Arrhenius representation of the dissociation rate (R) for isolated $[Cu(tma)_4]^{n-}$ compounds derived from analysis of STM data for low coverages at temperatures in the range 260–300 K. The corresponding energy barrier is determined to be $E_d = 0.31 \pm 0.08$ eV.

slope corresponds to the energy barrier for dissociation of the coordination compound (E_d). The linear fit of the data yields $E_d = 0.31 \pm 0.08$ eV. With the present system, the determined energy value is a combination of the contributions associated with the formation of coordination bonds and the repositioning of the involved elements (note that the value of the present energy barrier is smaller than the binding energy of related coordination compounds in the gas phase. The higher stability of the $[Cu_2(tma)_6]^{n-}$ configuration is understood to be a consequence of the increased number of coordination bonds involved and possibly an increased barrier for molecular rotations in this more densely packed arrangement (steric hindrance).

Our results show that single-molecule investigations can provide comprehensive insight into the evolution of coordination compounds, where several reacting species are involved. In view of the rich potential and wide application of metal–ligand interactions, it is suggested that such insight will be valuable in the future search for nanoscale elements on templates. More generally speaking, the observations reveal that the natural path of a multicomponent chemical reaction can be directly characterized and the corresponding energetics can be quantified.

Experimental Section

The sample preparation and characterization have been conducted in an ultrahigh vacuum (UHV) environment that provides well-defined conditions for the experiment. The UHV system (base pressure about 3×10^{-10} mbar) is equipped with a home-built variable-temperature UHV-STM described elsewhere (operational in the range of 40–800 K), as well as standard facilities for sample preparation and a quadrupole mass spectrometry analysis (QMS). The Cu(100) surface was cleaned by repeated cycles of Ar$^+$ sputtering and subsequent annealing (500 eV, 6 μA, 800 K), which allowed atomically flat terraces of up to 200 nm width separated by monatomic steps to be obtained. The STM experiments were performed in the constant current mode, with maximum bias voltages up to 2 V. Data were obtained starting in the temperature range 180–300 K. Commercially available tma (Fluka Chemie AG) in powder form was deposited by organic molecular beam epitaxy from a Knudsen-cell-type evaporator. The temperature of the cell was held constant at 460 K during the evaporation.

[1] a) J. K. Gimzewski, C. Joachim, *Science* **1999**, *283*, 1683–1688; b) C. Joachim, J. K. Gimzewski, A. Aviram, *Nature* **2000**, *408*, 541–548.

[2] a) M. Böhringer, K. Morgenstern, W. D. Schneider, R. Berndt, F. Mauri, A. De Vita, R. Car, *Phys. Rev. Lett.* **1999**, *83*, 324–327; b) M. Furukawa, H. Tanaka, K. Sugiara, Y. Sakata, T. Kawai, *Surf. Sci.* **2000**, *445*, L58–L63; c) T. Yokoyama, S. Yokoyama, T. Kamikado, Y. Okuno, S. Mashiko, *Nature* **2001**, *413*, 619–621.

[3] J. V. Barth, J. Weckesser, C. Cai, P. Gunter, L. Burgi, O. Jeandupeux, K. Kern, *Angew. Chem.* **2000**, *112*, 1285–1288; *Angew. Chem. Int. Ed.* **2000**, *39*, 1230–1234.

[4] A. Semenov, J. P. Spatz, M. Möller, J.-M. Lehn, B. Sell, D. Schubert, C. H. Weidl, U. S. Schubert, *Angew. Chem.* **1999**, *111*, 2701–2705; *Angew. Chem. Int. Ed.* **1999**, *38*, 2547–2550.

[5] D. G. Kurth, N. Severin, J. P. Rabe, *Angew. Chem.* **2002**, *114*, 3833–3835; *Angew. Chem. Int. Ed.* **2002**, *41*, 3681–3683.

[6] A. Werner, *Z. Anorg. Chem.* **1893**, *3*, 267–330.

[7] J.-M. Lehn, *Supramolecular Chemistry, Concepts and Perspectives*, VCH, Weinheim, **1995**.

[8] D. Philp, J. F. Stoddart, *Angew. Chem.* **1996**, *108*, 1242–1286; *Angew. Chem. Int. Ed.* **1996**, *35*, 1155–1196.

[9] B. J. Holliday, C. A. Mirkin, *Angew. Chem.* **2001**, *113*, 2076–2097; *Angew. Chem. Int. Ed.* **2001**, *40*, 2022–2043.

[10] R. C. Mehrotra, R. Bohra, *Metal Carboxylates*, Academic Press, London, **1983**.

[11] S. V. Kolotuchin, P. A. Thiessen, E. E. Fenlon, S. R. Wilson, C. J. Loweth, S. C. Zimmerman, *Chem. Eur. J.* **1999**, *5*, 2537–2547.

[12] A. Dmitriev, N. Lin, J. Weckesser, J. V. Barth, K. Kern, *J. Phys. Chem. B* **2002**, *106*(27), 6907–6912.

[13] C. C. Perry, S. Haq, B. G. Frederick, N. V. Richardson, *Surf. Sci.* **1998**, *409*, 512–520.

[14] The decisive role of atom evaporation from steps could be proven in the present case by the following experiments. In the first case, the step mobility was limited by step decoration with carbon monoxide which significantly delayed compound formation. In the second case, compound formation could be triggered by co-deposition of Cu or by raising the temperature.

[15] J. V. Barth, J. Weckesser, G. Trimarchi, M. Vladimirova, A. De Vita, C. Cai, H. Brune, P. Günter, K. Kern, *J. Am. Chem. Soc.* **2002**, *124*, 7991 – 8000.

[16] A. Doyle, J. Felcman, M. T. Gambardella, C. N. Verani, M. L. B. Tristão, *Polyhedron* **2000**, *19*, 2621 – 2627.

[17] P. R. Raithby, G. P. Shields, F. H. Allen W. D. S. Motherwell, *Acta Cryst. B* **2000**, *56*, 444 – 454.

[18] Movies showing the formation and decay of the coordination compounds in real space are shown at http://www.mpi-stutt-gart.mpg.de/kern/Res act/supmat 2.html.

[19] J. Lee, W. Ho, *Science* **1999**, *286*, 1719 – 1722.

[20] S.-W. Hla, L. Bartels, G. Meyer, K.-H. Rieder, *Phys. Rev. Lett.* **2000**, *85*, 2777 – 2780.

[21] Note, however, that single complexes are perfectly stable below 180 K, where molecular motion is frozen. No dissociation/association events are detected in the corresponding STM images, which demonstrates that the room-temperature dynamics of the complexes is not influenced by tip effects.

Low-Temperature Synthesis of Single-Crystal Germanium Nanowires by Chemical Vapor Deposition**

Dunwei Wang and Hongjie Dai*

Chemically derived nanowire materials have attracted much attention because of their interesting geometries, properties, and potential applications.[1–3] Various methods have been developed for synthesizing semiconducting nanowires including laser ablation,[2,3] physical vapor deposition under high temperatures,[3–7] and solvothermal growth under high pressures and moderate temperatures.[3,8–10] Chemical vapor deposition (CVD) has been extensively used for carbon nanotube growth,[11–13] but is much less explored for the synthesis of semiconductor nanowires, with the exception for silicon.[14,15]

Herein, we present the first synthesis of single-crystal germanium nanowires, prepared by the CVD of germane (GeH$_4$) at 275°C with Au nanocrystals as seed particles. Germanium is an important semiconducting electronic material with high carrier mobility and a band gap of approximately 0.6 eV. Nanowires of germanium were first reported by the group of Heath about ten years ago, synthesized by using a solvothermal approach.[8] Recently, laser ablation (820°C),[2] vapor transport (900–1100°C),[4,7,16] and solvothermal methods (300–400°C, 100 atm)[9] were used for growth. We show here that high-quality Ge nanowires are synthesized by a simple CVD process at 275°C under atmospheric pressure. This represents the mildest growth conditions for single-crystal nanowire synthesis. An efficient Ge feedstock

from GeH$_4$ and the low eutectic temperature of Ge–Au nanoclusters are the key factors that afford vapor-liquid-solid (VLS) growth of Ge nanowires at low temperatures. Further, we show that the CVD approach allows for patterned growth of Ge nanowires, which yields nanowires from well-defined patterned sites on surfaces.

We carried out CVD growth at 275°C under a 10 sccm (standard cubic centimeter) flow of GeH$_4$ (10% in He) in tandem with a 100 sccm flow of H$_2$ in a 2.5 cm furnace reactor (total gas pressure 1 atm) for 15 min. The SiO$_2$ substrate used in this work contained preformed Au nanocrystals (approximately 20 nm in diameter) deposited uniformly on the surface from a colloidal solution. The inset of Figure 1a shows an atomic force microscopy (AFM) image of the Au particles on a substrate, recorded before CVD. After the

[*] Prof. Dr. H. Dai, D. Wang
Department of Chemistry
Stanford University
Stanford, CA 94305 (USA)
Fax: (+1) 650-725-0259
E-mail: hdai@stanford.edu
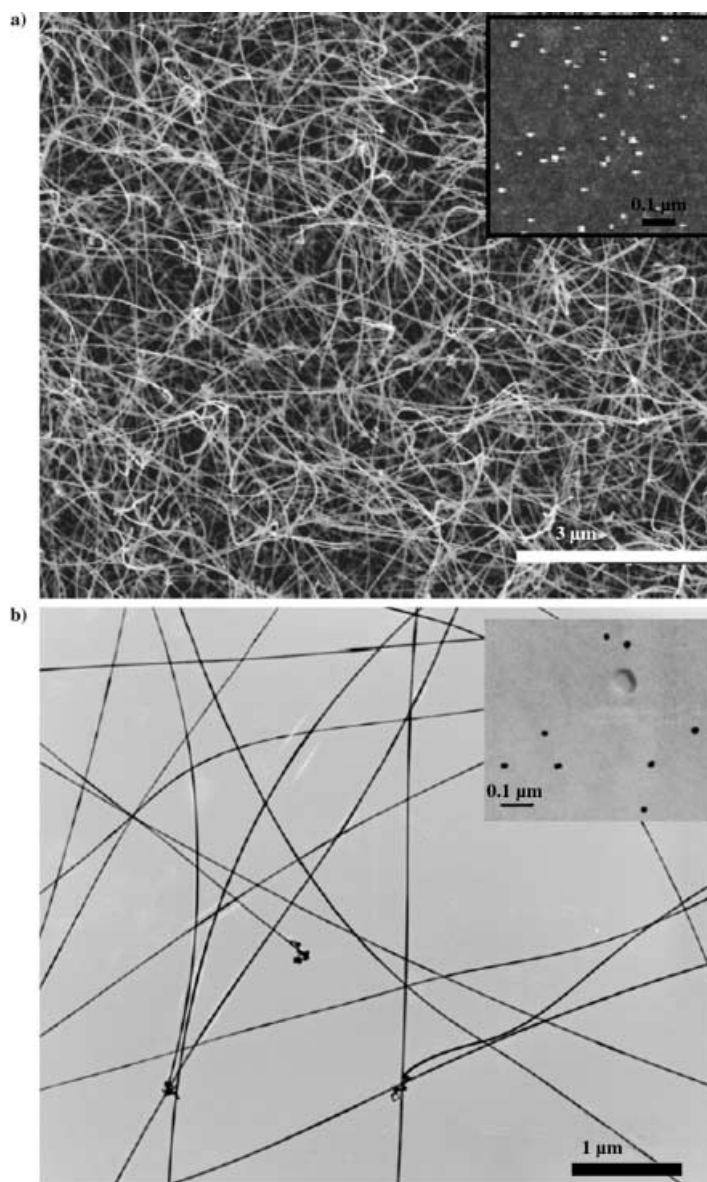
Figure 1. a) An SEM image of Ge nanowires synthesized by CVD at 275°C on a SiO$_2$/Si substrate. The inset shows an AFM image of Au nanoclusters on the substrate recorded prior to CVD; b) A TEM image of Ge nanowires synthesized by CVD on a SiO$_2$ film (approximately 10 nm thick; light background) supported on a TEM grid. The inset shows a TEM image of Au clusters (black dots) on SiO$_2$ recorded prior to CVD.